ARTICLES
https://doi.org/10.1038/s41557-021-00788-x

nature chemistry

A short peptide synthon for liquid–liquid phase separation

Manzar Abbas[1,2], Wojciech P. Lipiński[1,2], Karina K. Nakashima[1], Wilhelm T. S. Huck[1] and Evan Spruijt[1]✉

Liquid–liquid phase separation of disordered proteins has emerged as a ubiquitous route to membraneless compartments in living cells, and similar coacervates may have played a role when the first cells formed. However, existing coacervates are typically made of multiple macromolecular components, and designing short peptide analogues capable of self-coacervation has proven difficult. Here we present a short peptide synthon for phase separation, made of only two dipeptide stickers linked via a flexible, hydrophilic spacer. These small-molecule compounds self-coacervate into micrometre-sized liquid droplets at sub-millimolar concentrations, which retain up to 75 wt% water. The design is general and we derive guidelines for the required sticker hydrophobicity and spacer polarity. To illustrate their potential as protocells, we create a disulfide-linked derivative that undergoes reversible compartmentalization controlled by redox chemistry. The resulting coacervates sequester and melt nucleic acids, and act as microreactors that catalyse two different anabolic reactions yielding molecules of increasing complexity. This provides a stepping stone for new coacervate-based protocells made of single peptide species.

Compartmentalization is one of the central pillars of living systems and represents a key step in the emergence of extant life[1–3]. To understand how abiotic components could become organized in lifelike compartments with the ability to adapt and evolve, various types of protocells have been developed, including giant unilamellar vesicles, oil-in-water droplets, coacervates and colloidosomes[4–8]. Lipid vesicles are commonly seen as one of the most plausible predecessors of modern cells[5,8,9]. Their architecture strongly resembles the membranes found in all living cells and they can form spontaneously upon hydration from amphiphilic molecules. In addition, they have been shown to grow and split through swelling and physical disruption, respectively[10], which could be combined into a primitive cell cycle[8]. Peptide-based membranes or proteinoid capsules have been investigated as robust alternatives with a direct link to gene expression[11–13]. However, the lack in permeability of both lipid and amphiphilic peptide-based membranes to many polar building blocks of, for example, RNA and peptides poses problems for protometabolism and the flow of molecular information[11,14,15].

Membraneless coacervates are alternative compartments that are not hindered by these limitations[6,16]. Such compartments are formed spontaneously by liquid–liquid phase separation (LLPS) of mostly macromolecular components and are able to concentrate a wide range of solutes by partitioning. Coacervates are commonly divided into complex coacervates, formed by heterotypic interactions such as complexation of oppositely charged solutes, and simple coacervates, formed by homotypic interactions or segregation from solvent[17]. Both coacervate types retain, contrary to oil droplets, a large amount of water, because the constituting molecules contain a substantial fraction of polar residues, and they provide an environment in which ribozymes[18,19] and enzymes[20,21] can be active. In recent years, LLPS has also emerged as a ubiquitous route to the formation of membraneless compartments by intrinsically disordered proteins/regions (IDPs/IDRs) in living cells[22–24]. Their widespread occurrence and central roles suggest that prebiotic analogues of these intracellular condensates could have played a role in the emergence of cells. However, the fact that coacervates are typically made of large molecules and often require multiple interacting components is commonly regarded as a serious barrier for their relevance as protocells[6,16].

Coacervates made of nucleoside phosphates[16], short oligonucleotides[25] and short peptides[26,27] have been reported, but they all require oppositely charged species of higher molecular weight to form. Self-coacervation of single solute species has been reported for ampholytic block polypeptides with a length of about 50 amino acids involving heterotypic interactions[28], and for resilin-like polypeptides and elastin-like polypeptides of more than 100 amino acids involving mostly homotypic interactions[29]. The latter assemblies have also been called simple coacervates. However, designing much shorter peptide-based molecules that are capable of simple coacervation through homotypic interactions, analogous to disordered proteins undergoing phase separation in living cells such as FUS[30] and hnRNPA1[31], has proven difficult. Various motifs and interaction types underlying LLPS in IDPs/IDRs have been identified[32], but a minimal model system is still lacking.

In this article we present a short peptide synthon for LLPS. Our design is based on the sticker-and-spacer motif that was recently identified as an important characteristic of several phase-separating proteins[31,33,34], and provides a route to peptide-based protocells through self-coacervation of small molecules. We show that various dimers of aromatic or aliphatic dipeptides, linked by a hydrophilic spacer, can self-coacervate into micrometre-sized liquid droplets at submillimolar concentrations in a wide range of environmental conditions. Unlike previously reported supramolecular assemblies of dipeptides[35–38], these coacervate droplets are liquid, reversible, rich in water and responsive to pH, temperature and organic solutes, analogous to many intracellular condensates of disordered proteins. By using a disulfide-containing moiety to connect the dipeptide stickers together, we create versatile coacervate protocells made of a single component that can be formed and dissolved

[1]Institute for Molecules and Materials, Radboud University, Nijmegen, The Netherlands. [2]These authors contributed equally: M. Abbas, W.P. Lipiński. ✉e-mail: e.spruijt@science.ru.nl

reversibly by controlling the redox chemistry. These coacervate protocells further act as effective microcompartments that can take up a wide range of guests, including single-stranded DNA, RNA porphyrins and various organic dyes. Small RNA hairpins dehybridize upon uptake, while rotationally dynamic dyes such as thioflavins partly lose their rotational freedom inside the coacervates. Finally, we show how these peptide-based coacervates could play a role in the formation of molecules of increasing complexity, by acting as microreactors for different types of addition reactions. An aldol reaction and hydrazone formation occurred 44- and 13-fold faster, respectively, than the same reaction in aqueous solution because reactant sequestration and the local apolar environment inside the coacervates facilitates the reactions. These properties make coacervates of disulfide-coupled peptides promising and versatile protocells. The general design presented here could open the way for new protocells made of single peptide species, and model systems to obtain a fundamental insight into intracellular phase separation.

Results and discussion

Self-coacervation of peptide derivatives. Aromatic residues are known to be important for the phase-separation propensity of disordered proteins[30,31,39]. Recently, a sticker-and-spacer motif has been proposed that explains how separating these aromatic residues (stickers) by flexible regions of soluble residues (spacers) results in liquid condensates instead of solid aggregates[31]. However, a minimal design for protein LLPS, which could provide a starting point for single-component coacervate protocells, is still lacking. We hypothesized that linking two hydrophobic dipeptides together with a flexible, polar spacer could result in the formation of condensed liquid droplets if the association between the dipeptides was strong enough. Aromatic dipeptides such as phenylalanyl–phenylalanine (FF) have been widely studied for their ability to self-assemble into fibres and hydrogels[35–38]. However, these assemblies are often irreversible and do not yield liquid condensates capable of sequestering other solutes. By joining them together through a non-aromatic, flexible linker, a minimal motif consisting of two stickers and a spacer is created that can undergo simple coacervation above a critical association concentration. Similar sticker-and-spacer motifs have been used in other fields, such as polymer chemistry, to predict self-assembly and phase separation of block copolymers, for example[40,41].

In order to create a conjugate that could be used to develop tunable protocells, we selected a cystamine moiety to link two L-phenylalanyl-L-phenylalanine dipeptides together via their C termini (Fig. 1a and Supplementary Fig. 1). The disulfide bond of this linker allows for dynamic control over the assembly through redox chemistry[42]. Unlike FF dipeptides and most FF derivatives, the cystamine-conjugated derivative bis(phenylalanyl–phenylalanyl) cystamine (FFssFF) is completely soluble in water below pH 6 up to 15 mg ml^{-1} and no aggregation could be detected (Supplementary Fig. 6). However, when the pH was increased to 7 or higher, the solution of FFssFF became turbid (Supplementary Fig. 7). Microscopic investigation revealed the formation of condensed droplets with a typical size of 1–10 µm (Fig. 1b). These peptide-rich condensates are liquid, which is evident from their ability to fuse (Fig. 1c), spread and deform (Fig. 1d), and ultimately separate into a bulk phase after centrifugation (Fig. 1e), just like coacervates of polyelectrolytes or disordered proteins[16,26,27].

An important difference between these FFssFF droplets and other coacervates made of polyelectrolytes or proteins is the size of the constituent molecules. While synthetic polymers, RNA and intrinsically disordered proteins used to make coacervate droplets have a typical mass of more than 10 kDa, these peptide derivatives are small molecules with a molecular weight of less than 750 Da. Nonetheless, the droplets shown in Fig. 1 and Supplementary Fig. 6 are coacervates: they are condensed liquids containing the same solvent as the coexisting dilute phase (water) and enriched in at least one of the dissolved species (FFssFF)[43]. We determined the amount of water present in the coacervate droplets by separating them from the supernatant after centrifugation (Fig. 1e), and found that they indeed contain a substantial amount of water (75 ± 10% (wt/wt) at pH 8, Supplementary Information, section 2.3). In addition, the droplets contain a very high peptide concentration, reaching 1,000-fold higher concentrations than the surrounding dilute solution (Fig. 1f). Because of the high internal concentration, which results in a high viscosity and small capillary velocity (γ/η), coacervates of FFssFF do not coalesce easily, and the average droplet size of an emulsion of FFssFF coacervates increases only slowly over time (Supplementary Fig. 8). Eventually, the coacervate droplets undergo complete fusion, indicating that the peptides remain sufficiently mobile, and the droplets are liquid. We estimated the inverse capillary velocity from the coalescence of pairs of droplets to be 0.44 s µm^{-1} (Supplementary Information, section 3.2), which is slightly higher than previous reports for droplets of RGG IDRs[44], but lower than RNA-binding IDP Whi3[45], and suggests that FFssFF-based coacervates are comparable in viscosity to other IDPs.

A second difference between FFssFF coacervates and most other oligopeptide-based coacervate protocells studied so far[17] is that these types of peptide coacervates designed with a sticker-and-spacer architecture do not require combining two oppositely charged species, as is the case for complex coacervates[16,26,27]. The droplets shown in Fig. 1 form as a result of homotypic interactions between the apolar side groups of FFssFF, and are therefore called simple coacervates[46]. Measurements of FFssFF coacervation at different salt concentrations confirm that the ionic strength has a very small effect on the coacervation transition (Fig. 1g) and coacervate stability, while the phase transition is sensitive to pH, temperature and organic solutes (Supplementary Information, section 3.3). This situation is similar to the phase separation of aromatic-rich disordered proteins such as FUS[30] and hnRNPA1[31], although segregation from other cytosolic components is believed to play a role in the phase separation of IDRs/IDPs[47]. We finally investigated the role of hydrogen bonding in driving the phase transition and stabilizing the coacervates by titrating FFssFF with urea. We observed no sharp transition that indicated dissolution of the coacervates up to 5 M urea (Supplementary Fig. 14), in contrast to observations on fibrils of aromatic dipeptides such as FF, but only a gradual decrease in turbidity, consistent with the expected gradual decrease in refractive index mismatch. This indicates that hydrogen bonds only play a small role initially driving LLPS. An analogous situation exists for membraneless organelles, where LLPS is found to depend on charged patches and aromatic groups, while maturation and liquid-to-solid transition have been linked to hydrogen bonding[48]. Based on these similarities, the design shown in Fig. 1a could be regarded as a minimal model of the sticker-and-spacer motifs required for phase separation.

On the other hand, the FFssFF coacervates are fundamentally different from oil droplets in water that have been studied as protocell models[49,50], even though hydrophobic interactions underlie the formation of both. Coacervates, like the FFssFF droplets in Fig. 1, constitute a liquid phase that contains both peptides and water, which only exists when the peptide is dissolved in water. This situation is analogous to the formation of membraneless organelles from hydrated disordered proteins.

To explore the general nature of the design in Fig. 1a, we synthesized variants with different hydrophobic dipeptides (stickers, Table 1) and different hydrophilic linkers (spacers, Table 2), including a cystine linker. Compounds with amino acids carrying fewer hydrophobic side chains such as leucine ($\Delta G_{w\text{-}oct} = -5.2$ kJ mol^{-1} versus -7.1 kJ mol^{-1} for phenylalanine) formed clear liquid coacervate droplets, but required higher concentrations (Table 1 and Supplementary Information, section 3.4). Mixed compounds

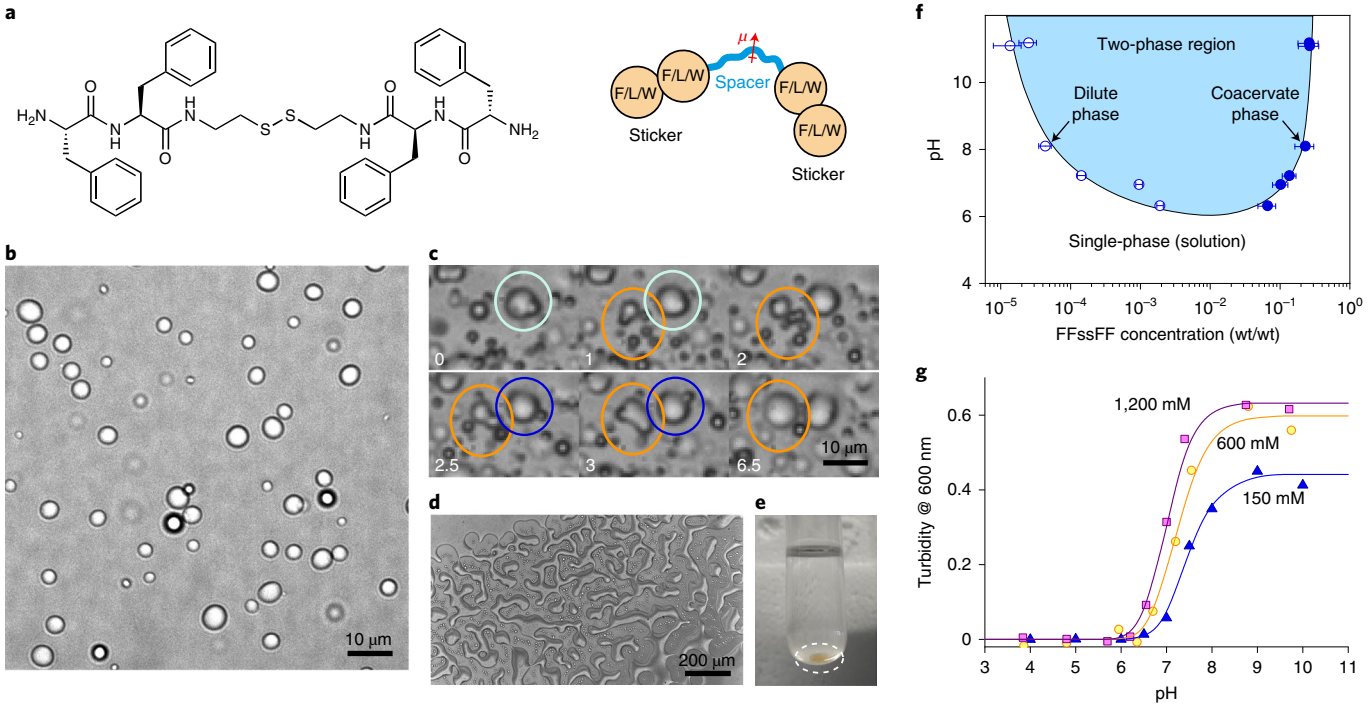

Fig. 1 | Liquid–liquid phase separation of cystamine-linked phenylalanine dipeptides. a, Structure of FFssFF and a schematic illustration of a synthon motif comprising two dipeptide stickers and a polar spacer. **b**, Microscope image of droplets of FFssFF (1 mg ml^{-1}, pH 8) after 5 min incubation. **c**, Fusion of FFssFF coacervate droplets (2 mg ml^{-1}, pH 8) (labels indicate time in minutes, coloured circles highlight fusion events). **d**, Wetting patterns formed by FFssFF coacervates (2 mg ml^{-1}, pH 8) on a glass surface. **e**, Bulk coacervate phase collected after centrifugation (3 mg ml^{-1}, pH 8, 4,000 r.c.f.). **f**, Phase diagram of FFssFF; the shaded area is the two-phase region in which coacervates are formed, the solid boundary line is drawn to guide the eye, and error bars indicate the measurement uncertainty in the solution and coacervate masses (see Supplementary Information, section 2.2). **g**, pH-triggered phase transition in FFssFF solutions (0.5 mg ml^{-1}) at different salt concentrations monitored by turbidity.

(FLssLF and LFssFL) had a critical coacervation concentration between the homodipeptide compounds LLssLL and FFssFF. For compounds with more hydrophobic side chains such as tryptophan ($\Delta G_{w\text{-}oct} = -8.7$ kJ mol^{-1}) the associations became too strong, and solid aggregates were found for WWssWW and the mixed compounds WFssFW and FWssWF. We confirmed the distinction between liquid coacervates and solid aggregates by determining the fluorescence recovery after photobleaching of five representative coacervates from Tables 1 and 2 (Supplementary Information, section 3.5). All liquid coacervates showed near-complete recovery with recovery half times between 20 and 100 s, while the derivatives forming solid aggregates showed no recovery. In addition, all liquid coacervates could take up the hydrophobic dye thioflavin T (ThT) by partitioning (Table 1).

Analysis of the condensation of different spacers revealed that polar and unstructured spacers with heteroatoms were all able to form coacervates (Table 2 and Supplementary Fig. 16). With the apolar 1,6-hexanediamine spacer, only aggregates were observed, while 2,2,4(2,4,4)-trimethyl-1,6-hexanediamine appeared to be at the boundary between coacervate and aggregate, showing tiny solvated globules attached together in a fractal-like aggregate. Taking the spacer's free energy of solvation and dipole moment as indicators of their ability to solubilize the stickers and keep the condensates in a hydrated, liquid state, we find a clear boundary between polar spacers with a zero or negative solvation free energy, which give rise to coacervates, and apolar spacers with a positive solvation free energy and limited solubility, which give rise to aggregates (Table 2 and Supplementary Fig. 5). Finally, compounds with a cystine spacer did not form coacervates, in agreement with cystine's low solubility and the propensity of cystine-containing peptides to form highly structured aggregates through β-sheet hydrogen bonding[51].

Altogether, we find that phase separation is the result of a balance between the solubilizing effect of one or more spacers, and the homotypic (hydrophobic) interactions between stickers. These guiding principles suggest that phase separation could be induced either by increasing the stickiness (hydrophobicity) of the stickers or decreasing the solvation free energy of the spacer. This is indeed what we observe for FFssFF solutions at pH 6.8 (Fig. 1g): at this pH FFssFF has too high a net charge to undergo LLPS. By increasing the salt concentration to 1.2 M, the homotypic interaction strength between stickers can be increased[52] and the electrostatic repulsion screened enough to induce phase separation. In brief, hydrophobic dipeptide stickers linked by an unstructured, polar spacer are minimal motifs for simple coacervation.

Redox reversibility of phase separation. We selected the phenylalanyl–phenylalanine peptide derivatives with a cystamine linker (FFssFF) to investigate the properties that make these coacervates attractive protocells in more detail. The disulfide bond allows direct control over coacervate formation by redox chemistry. By reducing the disulfide bond in FFssFF with tris(2-carboxyethyl)phosphine (TCEP), the peptide derivative is converted in two free thiols that are soluble in water, even at pH >7, and a turbid dispersion of coacervate droplets is converted into a clear solution (Fig. 2a). This transition is completely reversible by oxidation of the free thiols using oxidizing agents.

We monitored the redox-controlled phase transition in more detail using a turbidity titration. Figure 2b shows the complete disappearance of turbidity in a 1.0 mg ml^{-1} dispersion of FFssFF

Table 1 | Self-coacervation of different hydrophobic dipeptide stickers connected with a disulfide spacer

Sticker	Structure	Condensate appearance	$\Delta G_{w\text{-}oct,sticker}$ (kJ mol^{-1})[a]	Saturation concentration (mg ml^{-1})[b]	Partition coefficient ThT[c]	Aldol reaction rate constant (10^{-3} h^{-1})[d]
LL	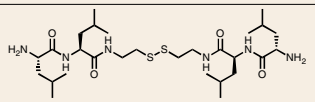	Coacervate	−10.4	2.1	18	340 ± 36[e]
LF	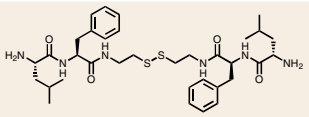	Coacervate	−12.3	0.054	6.3	52 ± 1.1
FL	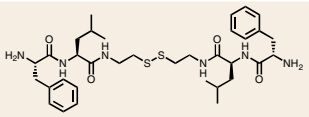	Coacervate	−12.3	0.066	9.1	55 ± 1.2
FF	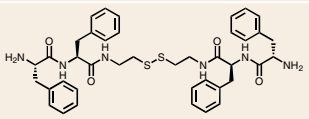	Coacervate	−14.2	0.018	30	46 ± 1.0
WF	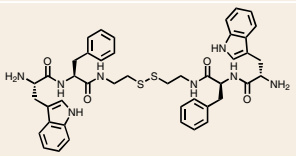	Aggregate	−15.8	0.002	ND	ND
FW	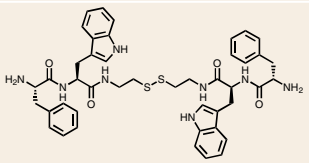	Aggregate	−15.8	0.002	ND	ND
WW	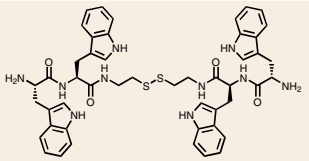	Aggregate	−17.4	0.001	ND	ND

ND, not determined. [a]Calculated as the sum of amino acid side chain transfer free energies. [b]HPLC analysis. [c]Confocal fluorescence microscopy analysis. [d]^{1}H NMR analysis of the aldol reaction between PNB and cyclohexanone (details in Supplementary Information, section 6.1). The equivalent rate without coacervates for FFssFF was $1.1 \pm 0.26 \times 10^{-3}$ h^{-1}. [e]Rate measured at a coacervate concentration of 3 mg ml^{-1} instead of 1 mg ml^{-1} because of the high solubility of LLssLL.

coacervates within 10 min upon addition of TCEP (19 mM final concentration). Mass spectrometry confirmed that all disulfides had been reduced to free FF-SH (Supplementary Information, section 4). Subsequent addition of $K_3Fe(CN)_6$ (45 mM final concentration) resulted in the formation of identical liquid droplets as before reduction (Fig. 2b) and reappearance of turbidity over 15 min. Mass spectrometry confirmed the formation of the original FFssFF. These regenerated coacervates could be completely dissolved again by reduction with TCEP, indicating that they have the same redox sensitivity as the originally formed coacervates. The turbidity after oxidation did not reach the same level as before the first reduction because the rate of coacervation is different. Initially, coacervates were formed very rapidly, within seconds, by increasing the pH of an acidic solution of FFssFF to 7. Coacervation by oxidation of thiols takes longer and some coacervates could have settled and adhered to the walls of the measuring chamber during that time. The same phenomenon is also observed when the turbidity decreases immediately after switching the pH (Fig. 2b,c).

The redox-induced coacervation is not limited to TCEP and ferricyanide. Any sufficiently strong reducing and oxidizing agent can drive the conversion. We carried out the same turbidity titration with DTT as reducing agent (Fig. 2c) and hydrogen peroxide as oxidizing agent (Supplementary Fig. 19), and found the same behaviour in both cases. These results show that oxidation of small dipeptide-conjugated thiols, such as FF-SH, under prebiotically relevant conditions can result in the efficient and spontaneous formation of protocellular compartments.

Selective partitioning of RNA, DNA and small molecule guests. One of the most important characteristics of coacervates and an argument for their potential relevance in the emergence of life is their ability to take up a wide variety of guest molecules and concentrate them to potentially high enough concentrations to facilitate reactions[6,16,21]. We determined the ability of the FFssFF coacervates to concentrate different guest molecules by fluorescence microscopy, as shown in Fig. 3. Aromatic fluorophores, including ThT (Fig. 3a,b), 4′,6-diamidino-2-phenylindole (DAPI, Fig. 3c), methylene blue (Fig. 3d) and SYBR Green (Fig. 3f) all became concentrated inside FFssFF coacervates, with apparent partition coefficients ($K = c_{droplet}/c_{solution}$) of 30, 35, 21 and 56, respectively, due to the different polarity inside the coacervates (Supplementary information 3.3). In the case of ThT, the strong fluorescence suggests that this fluorophore becomes rotationally restricted inside the coacervates by binding to the apolar peptide side groups, similar to its binding to

Table 2 | Self-coacervation of FF dipeptide stickers connected with different spacers

Spacer	Structure	Condensate appearance	Spacer solubility (mg ml^{-1})[a]	$\Delta G_{solv,spacer}$ (kJ mol^{-1})[b]	Dipole moment (D)[b]	Saturation concentration (mg ml^{-1})[c]	Partition coefficient ThT[d]	Aldol reaction rate constant (10^{-3} h^{-1})[e]
CC	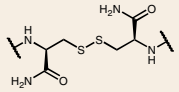	Aggregate	0.12	18 ± 1.3	0.2 ± 0.2	ND	ND	ND
CC[f]	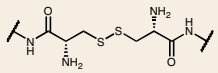	Aggregate	0.12	18 ± 1.3	0.2 ± 0.2	ND	ND	ND
c6	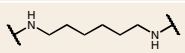	Aggregate	0.49	11 ± 2.0	2.0 ± 0.7	0.06	ND	ND
c8	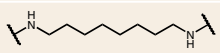	Aggregate	0.58	19 ± 1.2	1.9 ± 0.9	0.006	ND	ND
c6(Me)$_3$[g]	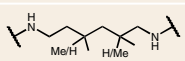	Aggregate/gel-like	>100	17 ± 1.6	2.2 ± 0.8	0.016	ND	ND
ss	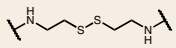	Coacervate	>100	−12 ± 6.0	4.8 ± 0.8	0.018	30	46 ± 1.0
s	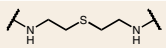	Coacervate	>100	−8.0 ± 3.1	3.3 ± 1.1	0.097	24	ND
o	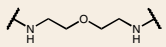	Coacervate	>100	−0.4 ± 2.8	2.9 ± 0.8	0.18	12.8	270 ± 10
eo$_2$[g]	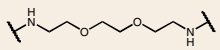	Coacervate	>100	0.9 ± 2.4	2.8 ± 0.7	0.45	9.3	ND

The boundary between compounds forming aggregates and coacervates coincides with a zero or negative solvation free energy and an increase in dipole moment (Supplementary Fig. 5). Standard deviations are based on six calculations (Supplementary Information, section 1.5). ND, not determined. [a]Information provided by supplier. [b]PM3 calculations using MolCalc (see Supplementary Methods). [c]HPLC analysis. [d]Confocal fluorescence microscopy analysis. [e]^{1}H NMR analysis of the aldol reaction between PNB and cyclohexanone (details in Supplementary Information, section 6.1). The equivalent rate without coacervates for FFssFF was 1.1 ± 0.26 × 10^{-3} h^{-1}. [f]Phenylalanyl–phenylalanine (FF) linked via the N terminus. [g]Mixture of stereoisomers.

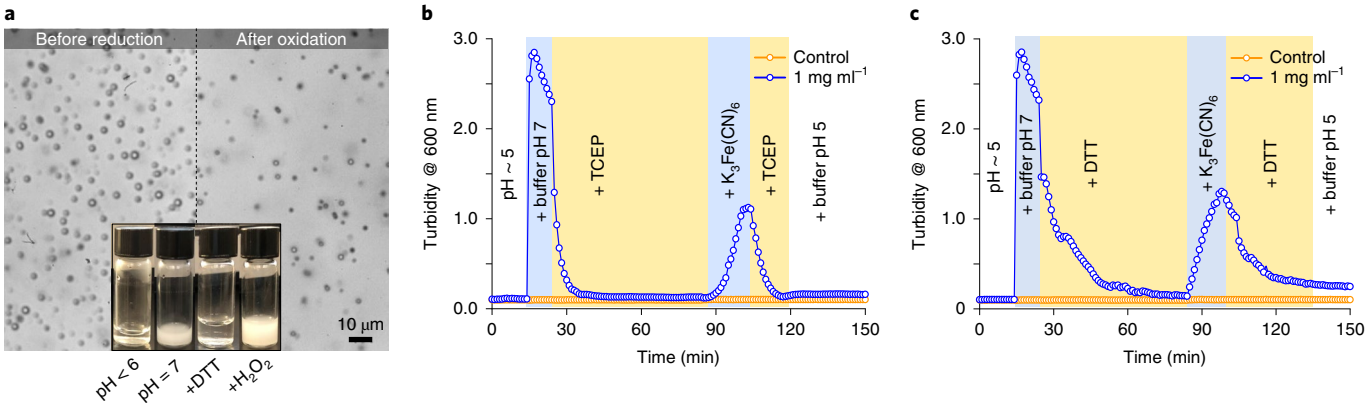

Fig. 2 | Reversible reduction and oxidation of FFssFF. a, FFssFF coacervate droplets before reduction and after oxidation. Inset: pictures of vials containing FFssFF (1 mg ml^{-1}) in various stages of the reduction and reoxidation: dissolved at low pH, phase separated at pH 7, dissolved after reduction and phase separated after oxidation. **b**, Kinetics of dissolution of FFssFF coacervates upon reduction with TCEP, and formation of coacervates through condensation upon oxidation with $K_3Fe(CN)_6$, as monitored by turbidity. **c**, Same as **b** but using DTT as reducing agent.

β-sheet structures in proteins. The fluorescence intensity of ThT in LLssLL coacervates was slightly lower ($K = 18$, Supplementary Fig. 20), as expected based on the weaker preference of ThT for the aliphatic isobutyl side chains of leucine[53]. Fluorescein was also taken up and concentrated inside FFssFF coacervates but to a much smaller extent (Fig. 3e, $K = 1.7$). The partition coefficients of these dyes are lower than in some polymeric coacervates[54], but the fact that various small molecules can still be concentrated is evidence for the potential utility of these coacervates in a protocell context.

Apart from small molecule fluorophores, these peptide-based coacervates also sequester longer nucleic acids. Figure 3g,h shows fluorescence microscope images of FFssFF coacervates that were incubated with 500 nM of ssDNA (43 nt) and ssRNA (24 nt), respectively. Both nucleic acids were concentrated and distributed evenly in the coacervate droplets ($K = 68$ and 75, respectively). This partitioning is weaker than in complex coacervates, where partial exchange with nucleotides inside the coacervates can lead to partition coefficients up to 10^5 (ref. [6]). To deduce the molecular basis of the partitioning of nucleic acids, we determined the partitioning of adenosine mono-, di- and triphosphate by HPLC (Supplementary Information, section 5.2). We found that the partition coefficient increases strongly with increasing number of phosphates, and

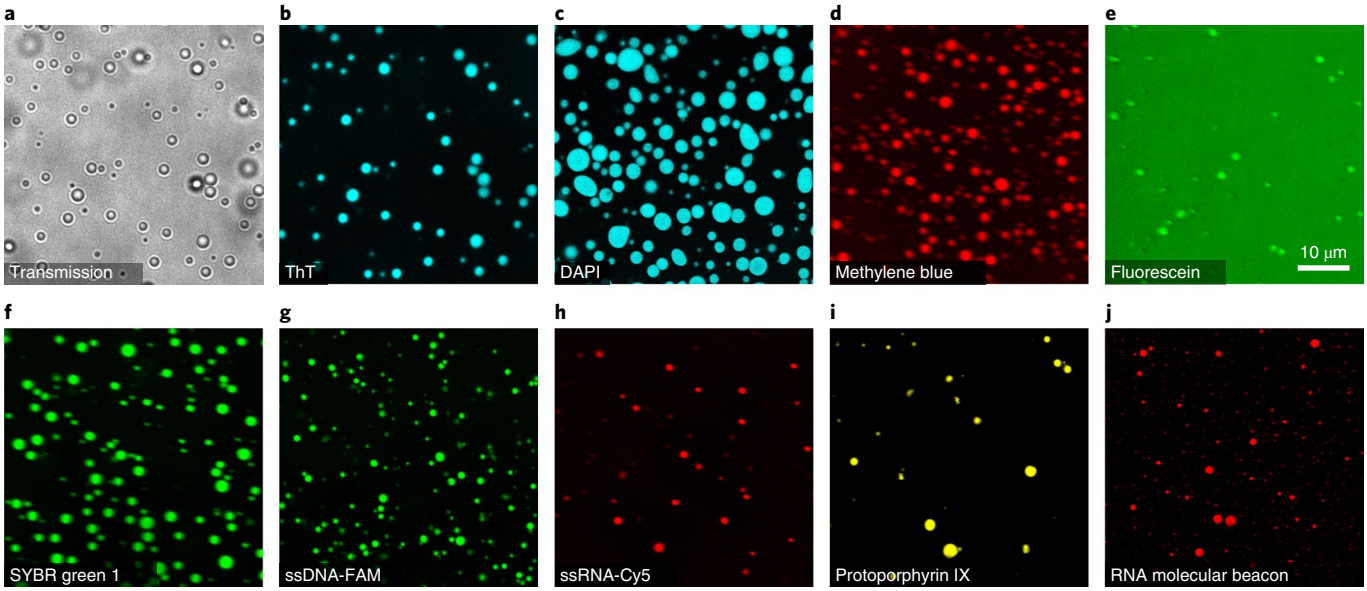

Fig. 3 | Partitioning of guest molecules in FFssFF coacervates. a, Bright-field image of FFssFF coacervates incubated with ThT. **b**, Confocal fluorescence image of ThT at the same position. **c**–**j**, Confocal fluorescence image of FFssFF coacervates incubated with DAPI (**c**), methylene blue (**d**), 5(6)-carboxyfluorescein (**e**), SYBR Green I (**f**), fluorescein amine-labelled ssDNA (43 nt) (**g**), Cy5-labelled ssRNA (24 nt) (**h**), protoporphyrin IX (**i**) and RNA molecular beacon (**j**). The scale bar shown **e** is the same for all images.

adenosine monophosphate exhibits no preferential partitioning ($K=1$). Therefore, we conclude that the partitioning of nucleotides and nucleic acids is dominated by interactions between the negatively charged phosphate groups and the amine groups on FFssFF. Finally, protoporphyrin IX, a prototypical anionic tetrapyrrole macrocycle and a precursor for haemoglobin and chlorophyll, was also concentrated in the FFssFF coacervates (Fig. 3i, $K=35$).

We then asked what influence the local physicochemical environment inside these peptide coacervates (Supplementary Information, sections 2 and 3) has on the stability of nucleic acid duplexes. A dehybridizing effect has previously been found for condensates formed by disordered proteins[55], while duplexes were stable inside condensates formed by short peptides[56] or oligonucleotides[57]. We incubated the coacervates with a short RNA hairpin with a 4 bp GC-stem designed to melt at 53 °C (50 mM NaCl, pH 7.4) and functionalized with a fluorophore–quencher pair[58]. We found that the hairpin was taken up and melted in the FFssFF coacervates (Fig. 3j), evidenced by the strong fluorescence signal compared to a control with 10-fold higher concentration of the same hairpin in buffer (Supplementary Fig. 22).

Enhanced rates of addition reactions in coacervate protocells. Inspired by the partitioning of both small molecules and large nucleic acids in FFssFF coacervates, we set out to investigate if they could act as microreactors[21] and enhance anabolic reactions yielding molecules of increasing complexity. First, we investigated the aldol reaction of an enol and an aldehyde, leading to C–C bond formation (Fig. 4a). This reaction is generally slow at neutral pH, but is known to be catalysed by proline and by various dipeptides, although it typically proceeds at an appreciable rate only if one of the substrates is added in large excess[59]. Aldol reactions play an important role in the synthesis of sugars, in the Krebs cycle and in various other protometabolic cycles[60]. We selected *p*-nitrobenzaldehyde (PNB) and cyclohexanone, which play no direct role in protometabolism, as substrates to enable monitoring the reaction kinetics directly by ^{1}H NMR. Without coacervates, no notable decrease in aldehyde concentration was observed in 48 h. Fitting of the integrated NMR data to a first-order rate equation for the aldehyde gave an apparent rate constant of $1.1\pm0.3\times10^{-3}\,h^{-1}$. By contrast, in the presence of FFssFF coacervates, complete disappearance of the aldehyde peak and formation of the aldol product was observed in approximately 48 h, with an apparent rate constant of $46\pm1\times10^{-3}\,h^{-1}$ (Fig. 4a). Other peptide derivatives in Tables 1 and 2 showed even faster conversion (Supplementary Fig. 23), with complete conversion in less than 15 h for LLssLL and FFoFF (apparent rate constants of $340\pm36\times10^{-3}\,h^{-1}$ and $270\pm10\times10^{-3}\,h^{-1}$, respectively). In a control reaction with peptides but without coacervates, no conversion was observed in 48 h (Supplementary Fig. 24), suggesting that the dipeptides alone do not catalyse the reaction sufficiently to observe complete conversion at the concentrations we used.

This 44- to 300-fold rate enhancement can thus be explained by concentration of the reactants inside the coacervates or the local apolar environment affecting the reaction barrier, or a combination of both, analogous to the rate enhancement in single-chain polymer nanoparticles[61]. When we performed a control reaction with tenfold higher concentration of both reactants, we did not observe a notable conversion (Supplementary Fig. 25), and the apparent rate constant of $2.1\pm0.4\times10^{-3}\,h^{-1}$ was still far from the observed rate in coacervates. We estimated the partition coefficients of PNB by absorbance, and found that it partitions only weakly in FFssFF coacervates ($K=3.5$), as expected for a small molecule. Partitioning in other coacervates from Tables 1 and 2 is probably even lower because FFssFF exhibited the highest apparent ThT partition coefficient. We therefore conclude that the rate enhancement is only partly caused by a higher local concentration of reactants. Another, important part is the result of the local (apolar) environment in the coacervates that facilitates the aldol reaction, like in catalysis, with an estimated decrease of the reaction energy barrier of 6.3 kJ mol^{-1} for FFssFF (Supplementary Information, section 6.1). The observed rate constants are the highest in the coacervates with the highest solubility (that is, the least hydrophobic stickers), which we believe can be attributed to a more pronounced exchange of peptides between these coacervates and the surrounding solution, which can take along substrates and products. A threshold sticker hydrophobicity is thus required to induce LLPS and form coacervates, but beyond

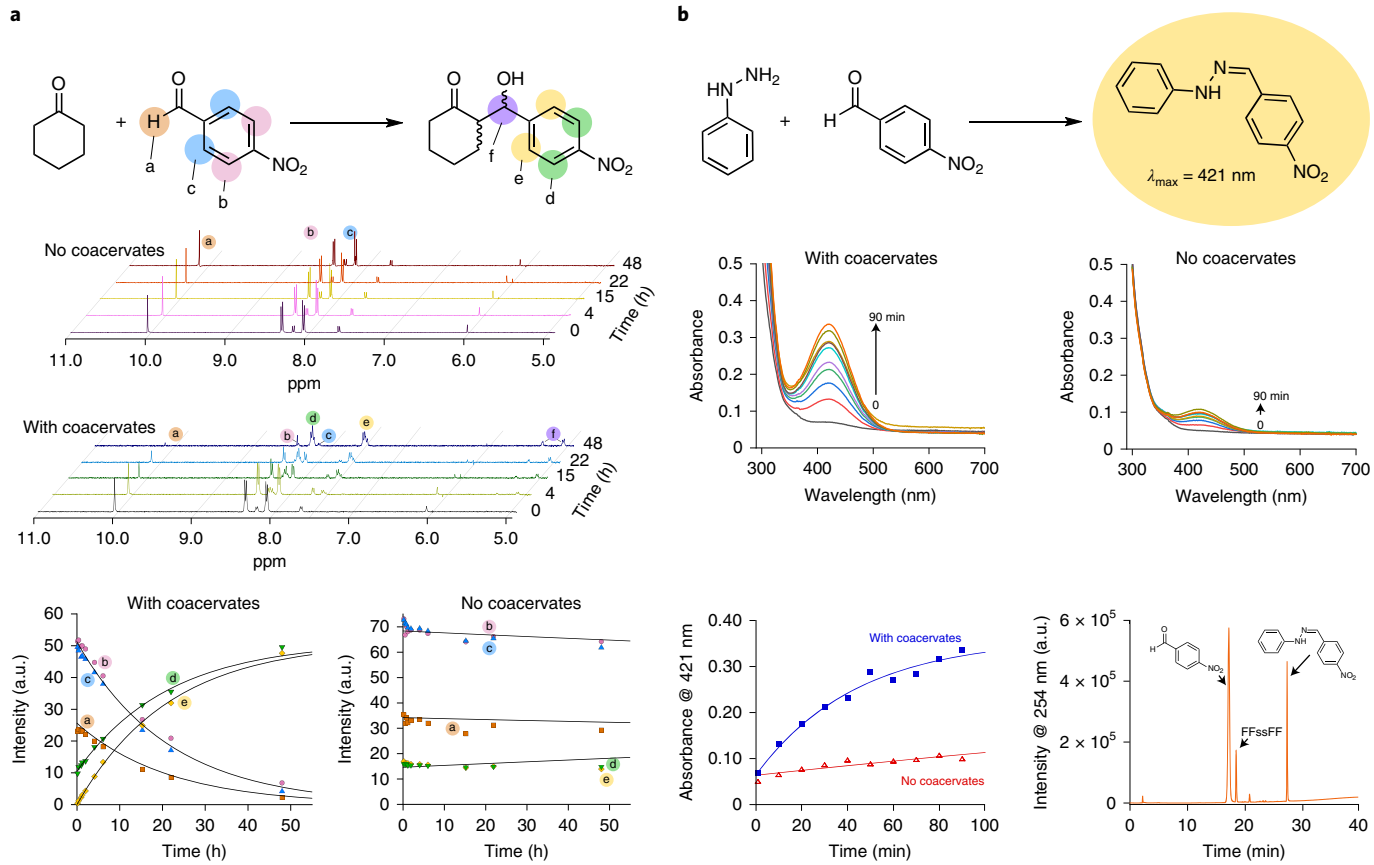

Fig. 4 | Enhanced rates of addition reactions in FFssFF coacervates. a, Aldol reaction between cyclohexanone and PNB in the absence and presence of FFssFF coacervates. From top to bottom: reaction scheme; ^{1}H NMR spectra of the reaction mixture without coacervates and with coacervates (peptide concentration, 0.2 mg ml^{-1}) taken after different incubation times; kinetics of aldol reaction in the absence and presence of coacervates (integrated NMR signals). Solid lines are simultaneous fits to all data using a first-order rate equation. **b**, Hydrazone formation between phenylhydrazine and PNB in the absence and presence of FFssFF coacervates. From top to bottom: reaction scheme; ultraviolet–visible spectra of the reaction mixture with FFssFF coacervates (peptide concentration, 0.2 mg ml^{-1}) and without FFssFF coacervates taken after different incubation times; kinetics of hydrazone formation in the presence and absence of coacervates (bottom left); HPLC analysis of the reaction mixture with coacervates after 90 min, showing peaks for the reactants and the product (bottom right). Solid lines in the kinetic plots are simultaneous fits to both data using a first-order rate equation with variable rate constant.

this threshold the stickers should be as soluble as possible for the best microreactor functionality.

We then looked at the hydrazone formation reaction between an aldehyde and a hydrazine, which is also slow at neutral pH without catalyst[62]. This reaction provides an effective way to form C–N bonds and is frequently used in dynamic combinatorial chemistry to create libraries of many possible conjugation products. We incubated 1 mM PNB and 0.2 mM phenylhydrazine in the absence and presence of FFssFF coacervates at room temperature, pH 7 (Fig. 4b). The hydrazone product of this reaction exhibits a clear absorption band at 421 nm[63], and its formation was confirmed by HPLC (Fig. 4b, bottom right, and Supplementary Fig. 26). We fitted the increase in absorbance to a first-order rate equation and found an apparent rate constant of $0.11 \pm 0.02\,h^{-1}$ for the reaction without coacervates, and $1.4 \pm 0.17\,h^{-1}$ in the presence of coacervates, a 12-fold enhancement. Like for the aldol reaction, this enhancement is explained by a combination of reactant concentration and the local apolar environment that facilitates condensation. Concentration of the reactants alone does not account for the observed rate enhancement: the partition coefficient of phenylhydrazine ($K = 1.8$) is even lower than that of PNB ($K = 3.5$), and when we repeated the experiment with fivefold higher concentrations of both the aldehyde and hydrazine, we observed an apparent rate constant of $0.69 \pm 0.11\,h^{-1}$ (Supplementary Fig. 27), which is still more than twofold lower than inside the coacervates. Similar to the situation with the aldol reaction, the hydrazone formation is only partly caused by a higher local concentration of reactants. An important contribution to the rate enhancement comes from an apparent lowering of reaction barrier for hydrazone formation by 1.6 kJ mol^{-1} inside the FFssFF coacervate protocells.

Finally, we explored the ability of FFssFF coacervates to undergo a reaction that modifies the state and stability of the compartments itself. To illustrate the potential utility of these compartments as protocells, we selected amino thioacids as potential prebiotic precursors of amino acids, which can form peptides by oxidative ligation. When we incubated FFssFF coacervates with phenylalanine thioacid (Phe-SH) in a 5:1 ratio, we observed the formation of the ligation product FFFssFF after 24 h, together with the appearance of gel-like agglomerates of solidified coacervates, which were no longer soluble by decreasing the pH (Supplementary Fig. 28). These results show that peptide-based coacervates can not only act as microreactors, but that they can also be transformed by in situ reactions into condensates with enhanced stability. This opens a range of possibilities for coacervate-based protocells made of single peptide species.

Conclusions

We have developed a new class of short peptide derivatives, which represent a synthon for LLPS. When dissolved in water, these

small-molecule compounds self-coacervate into stable liquid droplets that contain up to 75 wt% water upon increasing the temperature or pH. The peptide derivatives were designed after a recent sticker-and-spacer model for protein-phase separation[31] and represent the minimal motif required for phase separation. The derivatives consist of two hydrophobic dipeptide stickers, linked together by a flexible hydrophilic spacer. We have identified guidelines for sticker hydrophobicity and spacer polarity that define the boundary between dynamic liquids and aggregated solids. For intracellular protein condensates, precisely this boundary is believed to separate healthy organelles from disease states[23], and the minimal LLPS motif presented here could open the way for the development of model systems to systematically study the molecular principles underlying the liquid-to-solid transition. An important first step would be to use bioinformatics tools and computer-aided peptide design to identify minimal unstructured peptide sequences to replace the pseudopeptide linker in our synthon[64].

Moreover, the minimal sticker-and-spacer coacervates we created are attractive protocell models based on their structural simplicity and unique chemical properties. We have used FFssFF, a disulfide-linked derivative with two aromatic dipeptides, to show for the first time that a single small-molecule compound can form effective microcompartments by self-coacervation at submillimolar concentrations. We were able to control the formation of these protocells using redox chemistry, and to sequester and melt nucleic acids inside these coacervates. Finally, the coacervates can act as catalytic microreactors for two widely used addition reactions. The rate enhancement of aldol and hydrazone formation reaction can only be explained by a combination of increased concentration and a lowering of the reaction barrier due to the local apolar environment, similar to what happens in micellar catalysis[65]. These results are a proof of principle of coacervate catalysis, and provide a stepping stone for the development of a wide range of new protocells with catalytic properties made of single peptide species.

Online content

Any methods, additional references, Nature Research reporting summaries, source data, extended data, supplementary information, acknowledgements, peer review information; details of author contributions and competing interests; and statements of data and code availability are available at https://doi.org/10.1038/s41557-021-00788-x.

Received: 17 July 2020; Accepted: 13 August 2021;
Published online: 11 October 2021

References

1. Koshland, D. E. Jr. Special essay: The seven pillars of life. *Science* **295**, 2215–2216 (2002).
2. Yewdall, N. A., Mason, A. F. & van Hest, J. C. M. The hallmarks of living systems: towards creating artificial cells. *Interface Focus* **8**, 20180023 (2018).
3. Mann, S. Systems of creation: the emergence of life from nonliving matter. *Acc. Chem. Res.* **45**, 2131–2141 (2012).
4. Cronin, L. & Walker, S. I. Beyond prebiotic chemistry. *Science* **352**, 1174–1175 (2016).
5. Dzieciol, A. J. & Mann, S. Designs for life: protocell models in the laboratory. *Chem. Soc. Rev.* **41**, 79–85 (2012).
6. Poudyal, R. R., Pir Cakmak, F., Keating, C. D. & Bevilacqua, P. C. Physical principles and extant biology reveal roles for RNA-containing membraneless compartments in origins of life chemistry. *Biochemistry* **57**, 2509–2519 (2018).
7. Toparlak, O. D. & Mansy, S. S. Progress in synthesizing protocells. *Exp. Biol. Med.* **244**, 304–313 (2019).
8. Kurihara, K. et al. A recursive vesicle-based model protocell with a primitive model cell cycle. *Nat. Commun.* **6**, 8352 (2015).
9. Blain, J. C. & Szostak, J. W. Progress toward synthetic cells. *Annu. Rev. Biochem.* **83**, 615–640 (2014).
10. Hanczyc, M. M., Fujikawa, S. M. & Szostak, J. W. Experimental models of primitive cellular compartments: encapsulation, growth, and division. *Science* **302**, 618–622 (2003).
11. Vogele, K. et al. Towards synthetic cells using peptide-based reaction compartments. *Nat. Commun.* **9**, 3862 (2018).
12. Schreiber, A., Huber, M. C. & Schiller, S. M. Prebiotic protocell model based on dynamic protein membranes accommodating anabolic reactions. *Langmuir* **35**, 9593–9610 (2019).
13. Rahman, Md. M., Ueda, M., Hirose, T. & Ito, Y. Spontaneous formation of gating lipid domain in uniform-size peptide vesicles for controlled release. *J. Am. Chem. Soc.* **140**, 17956–17961 (2018).
14. Monnard, P.-A. & Deamer, D. W. Membrane self-assembly processes: steps toward the first cellular life. *Anat. Rec.* **268**, 196–207 (2002).
15. Litschel, T. et al. Freeze–thaw cycles induce content exchange between cell-sized lipid vesicles. *New J. Phys.* **20**, 055008 (2018).
16. Koga, S., Williams, D. S., Perriman, A. W. & Mann, S. Peptide–nucleotide microdroplets as a step towards a membrane-free protocell model. *Nat. Chem.* **3**, 720–724 (2011).
17. Abbas, M., Lipiński, W. P., Wang, J. & Spruijt, E. Peptide-based coacervates as biomimetic protocells. *Chem. Soc. Rev.* **50**, 3690–3705 (2021).
18. Drobot, B. et al. Compartmentalised RNA catalysis in membrane-free coacervate protocells. *Nat. Commun.* **9**, 3643 (2018).
19. Poudyal, R. R. et al. Template-directed RNA polymerization and enhanced ribozyme catalysis inside membraneless compartments formed by coacervates. *Nat. Commun.* **10**, 490 (2019).
20. Nakashima, K. K., Baaij, J. F. & Spruijt, E. Reversible generation of coacervate droplets in an enzymatic network. *Soft Matter* **14**, 361–367 (2018).
21. Love, C. et al. Reversible pH-responsive coacervate formation in lipid vesicles activates dormant enzymatic reactions. *Angew. Chem. Int. Ed.* **59**, 5950–5957 (2020).
22. Boeynaems, S. et al. Protein phase separation: a new phase in cell biology. *Trends Cell Biol.* **28**, 420–435 (2018).
23. Shin, Y. & Brangwynne, C. P. Liquid phase condensation in cell physiology and disease. *Science* **357**, eaaf4382 (2017).
24. Banani, S. F., Lee, H. O., Hyman, A. A. & Rosen, M. K. Biomolecular condensates: organizers of cellular biochemistry. *Nat. Rev. Mol. Cell Biol.* **18**, 285–298 (2017).
25. Yin, Y. et al. Non-equilibrium behaviour in coacervate-based protocells under electric-field-induced excitation. *Nat. Commun.* **7**, 10658 (2016).
26. Perry, S. L. et al. Chirality-selected phase behaviour in ionic polypeptide complexes. *Nat. Commun.* **6**, 1–8 (2015).
27. Aumiller, W. M. & Keating, C. D. Phosphorylation-mediated RNA/peptide complex coacervation as a model for intracellular liquid organelles. *Nat. Chem.* **8**, 129–137 (2016).
28. Madinya, J. J., Chang, L.-W., Perry, S. L. & Sing, C. E. Sequence-dependent self-coacervation in high charge-density polyampholytes. *Mol. Syst. Des. Eng.* **5**, 632–644 (2020).
29. Simon, J. R., Carroll, N. J., Rubinstein, M., Chilkoti, A. & López, G. P. Programming molecular self-assembly of intrinsically disordered proteins containing sequences of low complexity. *Nat. Chem.* **9**, 509–515 (2017).
30. Murthy, A. C. et al. Molecular interactions underlying liquid–liquid phase separation of the FUS low-complexity domain. *Nat. Struct. Mol. Biol.* **26**, 637–648 (2019).
31. Martin, E. W. et al. Valence and patterning of aromatic residues determine the phase behavior of prion-like domains. *Science* **367**, 694–699 (2020).
32. Gomes, E. & Shorter, J. The molecular language of membraneless organelles. *J. Biol. Chem.* **294**, 7115–7127 (2019).
33. Wang, J. et al. A molecular grammar governing the driving forces for phase separation of prion-like RNA binding proteins. *Cell* **174**, 688–699.e16 (2018).
34. Choi, J.-M., Holehouse, A. S. & Pappu, R. V. Physical principles underlying the complex biology of intracellular phase transitions. *Annu. Rev. Biophys.* **49**, 107–133 (2020).
35. Reches, M. & Gazit, E. Formation of closed-cage nanostructures by self-assembly of aromatic dipeptides. *Nano Lett.* **4**, 581–585 (2004).
36. Adler-Abramovich, L. & Gazit, E. The physical properties of supramolecular peptide assemblies: from building block association to technological applications. *Chem. Soc. Rev.* **43**, 6881–6893 (2014).
37. Chen, C., Liu, K., Li, J. & Yan, X. Functional architectures based on self-assembly of bio-inspired dipeptides: structure modulation and its photoelectronic applications. *Adv. Colloid Interface Sci.* **225**, 177–193 (2015).
38. Yuan, C. et al. Nucleation and growth of amino acid and peptide supramolecular polymers through liquid–liquid phase separation. *Angew. Chem. Int. Ed.* **58**, 18116–18123 (2019).
39. Brady, J. P. et al. Structural and hydrodynamic properties of an intrinsically disordered region of a germ cell-specific protein on phase separation. *Proc. Natl Acad. Sci. USA* **114**, E8194–E8203 (2017).
40. Sprakel, J., Besseling, N. A. M., Cohen Stuart, M. A. & Leermakers, F. A. M. Phase behavior of flowerlike micelles in a SCF cell model. *Eur. Phys. J. E* **25**, 163–173 (2008).
41. Srivastava, S. et al. Gel phase formation in dilute triblock copolyelectrolyte complexes. *Nat. Commun.* **8**, 14131 (2017).

42. Zhang, X., Malhotra, S., Molina, M. & Haag, R. Micro- and nanogels with labile crosslinks—from synthesis to biomedical applications. *Chem. Soc. Rev.* **44**, 1948–1973 (2015).
43. Bungenberg de Jong, H. G. & Kruyt, H. R. Coacervation (partial miscibility in colloid systems). *Proc. Neth. Acad. Sci.* **32**, 849–856 (1929).
44. Schuster, B. S. et al. Identifying sequence perturbations to an intrinsically disordered protein that determine its phase-separation behavior. *Proc. Natl Acad. Sci. USA* **117**, 11421–11431 (2020).
45. Zhang, H. et al. RNA controls polyQ protein phase transitions. *Mol. Cell* **60**, 220–230 (2015).
46. Kaminker, I. et al. Simple peptide coacervates adapted for rapid pressure-sensitive wet adhesion. *Soft Matter* **13**, 9122–9131 (2017).
47. André, A. A. M. & Spruijt, E. Liquid–liquid phase separation in crowded environments. *Int. J. Mol. Sci.* **21**, 5908 (2020).
48. Shen, Y. et al. Biomolecular condensates undergo a generic shear-mediated liquid-to-solid transition. *Nat. Nanotechnol.* **15**, 841–847 (2020).
49. Gutierrez, J. M. P., Hinkley, T., Taylor, J. W., Yanev, K. & Cronin, L. Evolution of oil droplets in a chemorobotic platform. *Nat. Commun.* **5**, ncomms6571 (2014).
50. Tena-Solsona, M., Wanzke, C., Riess, B., Bausch, A. R. & Boekhoven, J. Self-selection of dissipative assemblies driven by primitive chemical reaction networks. *Nat. Commun.* **9**, 2044 (2018).
51. Cashman, T. J. & Linton, B. R. β-Sheet hydrogen bonding patterns in cystine peptides. *Org. Lett.* **9**, 5457–5460 (2007).
52. Bogunia, M. & Makowski, M. Influence of ionic strength on hydrophobic interactions in water: dependence on solute size and shape. *J. Phys. Chem. B* **124**, 10326–10336 (2020).
53. Biancalana, M., Makabe, K., Koide, A. & Koide, S. Molecular mechanism of thioflavin-T binding to the surface of β-rich peptide self-assemblies. *J. Mol. Biol.* **385**, 1052–1063 (2009).
54. Zhao, M. et al. Partitioning of small molecules in hydrogen-bonding complex coacervates of poly(acrylic acid) and poly(ethylene glycol) or pluronic block copolymer. *Macromolecules* **50**, 3818–3830 (2017).
55. Nott, T. J., Craggs, T. D. & Baldwin, A. J. Membraneless organelles can melt nucleic acid duplexes and act as biomolecular filters. *Nat. Chem.* **8**, 569–575 (2016).
56. Cakmak, F. P., Choi, S., Meyer, M. O., Bevilacqua, P. C. & Keating, C. D. Prebiotically-relevant low polyion multivalency can improve functionality of membraneless compartments. *Nat. Commun.* **11**, 5949 (2020).
57. Vieregg, J. R. et al. Oligonucleotide–peptide complexes: phase control by hybridization. *J. Am. Chem. Soc.* **140**, 1632–1638 (2018).
58. Sokolova, E. et al. Enhanced transcription rates in membrane-free protocells formed by coacervation of cell lysate. *Proc. Natl Acad. Sci. USA* **110**, 11692–11697 (2013).
59. Luppi, G. et al. Dipeptide-catalyzed asymmetric aldol condensation of acetone with (*N*-alkylated) isatins. *J. Org. Chem.* **70**, 7418–7421 (2005).
60. Springsteen, G., Yerabolu, J. R., Nelson, J., Rhea, C. J. & Krishnamurthy, R. Linked cycles of oxidative decarboxylation of glyoxylate as protometabolic analogs of the citric acid cycle. *Nat. Commun.* **9**, 91 (2018).
61. Huerta, E., van Genabeek, B., Stals, P. J. M., Meijer, E. W. & Palmans, A. R. A. A modular approach to introduce function into single-chain polymeric nanoparticles. *Macromol. Rapid Commun.* **35**, 1320–1325 (2014).
62. Dirksen, A., Dirksen, S., Hackeng, T. M. & Dawson, P. E. Nucleophilic catalysis of hydrazone formation and transimination: implications for dynamic covalent chemistry. *J. Am. Chem. Soc.* **128**, 15602–15603 (2006).
63. Li, J. et al. Determination of residual phenylhydrazines in drug substances by high-performance liquid chromatography with pre-column derivatization. *Anal. Methods* **11**, 6146–6152 (2019).
64. Frederix, P. W. J. M. et al. Exploring the sequence space for (tri-)peptide self-assembly to design and discover new hydrogels. *Nat. Chem.* **7**, 30–37 (2015).
65. Serrano-Luginbühl, S., Ruiz-Mirazo, K., Ostaszewski, R., Gallou, F. & Walde, P. Soft and dispersed interface-rich aqueous systems that promote and guide chemical reactions. *Nat. Rev. Chem.* **2**, 306–327 (2018).

Methods

Synthesis. All peptide derivatives were synthesized via solution-phase synthesis methods. Full details of the synthesis and characterizations are given in the Supplementary Information.

Coacervation. The lyophilized powder of dipeptide derivatives was dissolved in Milli-Q water. The pH of the homogeneous solution of peptide derivatives was in the range of 5–6 depending on the concentration of the peptide. The coacervation/aggregation was triggered by increasing the pH to 7 using 1 µl of 0.2 M NaOH solution or 5 µl of 100 mM phosphate/Tris/TEAB buffer for each 100 µl solution of peptide. The milky colour appeared immediately and coacervation was confirmed by bright-field microscopy (Olympus IX71 inverted microscope).

Turbidity. All turbidity-based titrations were performed on a Tecan Spark multimode plate reader with a built-in spectrophotometer and automated injector. We use turbidity as an indicator of LLPS for samples in which liquid droplets have been confirmed by optical microscopy. We used 600 nm as the wavelength for all turbidity measurements, and all measurements were performed at room temperature (21 ± 2 °C), unless stated otherwise. Titrations were carried out in triplicate and the titrant concentration was chosen such that the added volume did not exceed 10% of the original volume, except for acetonitrile and L-phenylalanine methyl ester (Phe-OMe) titrations. Turbidity was recorded after shaking the sample for 5 s following each addition. A well with the same volume of buffer was used as blank.

Partitioning experiments. For partitioning of guest molecules we used a 1 mg ml^{-1} stock solution of FFssFF at pH <6. We prepared 1 mM stock solutions of the dye molecules, 10 µM stock solutions of ssDNA-FAM (140 ng µl^{-1}), ssRNA-Cy5 (85 ng µl^{-1}) and RNA hairpin (100 ng µl^{-1}), and a saturated solution of protoporphyrin IX in Milli-Q water. Twenty microlitres of FFssFF stock solution was mixed with 2 µl of a 100 mM buffer solution pH 7.5 (Tris) to induce coacervation. After 1 min, 2 µl of the dye stock solutions or 1 µl of the nucleic acid stock solutions was added and mixed with the coacervates by pipetting. The mixtures were incubated for 30 min, and after incubation 10 µl of the mixture was applied on a cover glass (number 1.5H) and imaged directly using a CSU X-1 Yokogawa spinning disc confocal system on an Olympus IX81 inverted microscope, or a Leica TCS Sp8X confocal microscope (HC PL APO ×100/1.40 (oil) CS2 objective).

Microreactor experiment. We performed two chemical reactions to test the catalytic activity of FFssFF coacervates.

(1) The aldol reaction between 4-nitrobenzaldehyde and cyclohexanone was performed with and without FFssFF coacervates at pH 9. Fresh stock solutions of 4-nitrobenzaldehyde (1.0 M) and cyclohexanone (1.0 M) in DMSO-d_6 and FFssFF (1 mg ml^{-1}) in D_2O were prepared. To induce coacervation, 2 µl of NaOD (0.87 M in D_2O) was added to 1 ml of the peptide solution, followed by the addition of 5 µl of dioxane in D_2O (2 M) as internal standard, and 10 µl of 4-nitrobenzaldehyde. All components were mixed well in a 5 mm NMR tube. A prescan was performed to calculate the exact concentration of aldehyde in the reaction mixture. Then, 20 µl of cyclohexanone was added into the NMR tube to initiate the aldol reaction, everything was mixed and ^{1}H NMR spectra of the reaction mixture were recorded at regular time intervals.

(2) Hydrazone formation between phenylhydrazine and 4-nitrobenzaldehyde was carried out with and without FFssFF coacervates at pH 8.5, which was set using 10 mM phosphate buffer saline (with 137 mM NaCl and 2.7 mM KCl). Fresh stock solutions of 4-nitrobenzaldehyde (300 mM) and phenylhydrazine (60 mM) were prepared in DMF, and a stock solution of FFssFF (2 mg ml^{-1}) was prepared in Milli-Q water. Coacervation was induced by mixing 300 µl of the FFssFF solution with 300 µl phosphate buffer saline (10 mM, pH 8.5). Then, 600 µl of that suspension was mixed with 2 µl of the phenylhydrazine solution and 2 µl of the 4-nitrobenzaldehyde solution by vortexing. Aliquots (50 µl) were taken from the reaction mixture every 10 min, and the coacervates were dissolved by mixing with an equal volume of acetonitrile, yielding a clear solution. Absorption spectra of the samples were recorded on a Jasco V-630 ultraviolet–visible spectrophotometer. The remaining details about the control experiments of addition reactions can be found in the Supplementary Information.

Statistics and reproducibility. Synthesis of the coacervate-forming compounds in Tables 1 and 2 was repeated at least three times, and similar coacervates were obtained with each batch (Fig. 1b–e). Titration experiments of coacervate dispersions with salt, acid/base, co-solutes and oxidizing and reducing agents (Figs. 1f,g and 2b,c) were all repeated at least three times with similar results. Guest molecule encapsulation experiments (Fig. 3) were repeated at least two times. Aldol and hydrazone reactions in coacervate dispersions were repeated at least three times (Fig. 4).

Data availability

All data supporting the findings of this study are available within the article and in the Supplementary Information and Data files. Source data are provided with this paper.

Acknowledgements

This project has received funding from the European Research Council (ERC) under the European Union's Horizon 2020 research and innovation programme under grant agreement number 851963, and from the Netherlands Organization for Scientific Research (NWO-Startup to E.S.). M.A. gratefully acknowledges a Marie Skłodowska Curie Individual Fellowship (project number 839177).

Author contributions

M.A. and E.S. conceived the idea and designed the experiments. M.A. and W.P.L. synthesized the peptide derivatives and performed their analysis. M.A. performed redox, microscopy and microreactor experiments. K.K.N. performed microscopy experiments with FFssFF. All authors discussed the results and interpreted data. M.A., E.S. and W.T.S.H. wrote the manuscript.

Competing interests

The authors declare no competing interests.

Additional information

Supplementary information The online version contains supplementary material available at https://doi.org/10.1038/s41557-021-00788-x.

Correspondence and requests for materials should be addressed to Evan Spruijt.

Peer review information *Nature Chemistry* thanks Samrat Mukhopadhyay and the other, anonymous, reviewer(s) for their contribution to the peer review of this work.

Reprints and permissions information is available at www.nature.com/reprints.